Lethaia
AN INTERNATIONAL JOURNAL OF PALAEONTOLOGY AND STRATIGRAPHY

Diopatra cuprea worm burrow parchment: a cautionary tale of infaunal surface reactivity

KURT O. KONHAUSER, WEIDUO HAO, YUHAO LI, KONSTANTIN VON GUNTEN, BRENDAN A. BISHOP, DANIEL S. ALESSI, LIDYA G. TARHAN, BRENNAN O'CONNELL, LESLIE J. ROBBINS, NOAH J. PLANAVSKY AND MURRAY K. GINGRAS

LETHAIA

Konhauser, K.O., Hao, W., Li, Y., von Gunten, K., Bishop, B.A., Alessi, D.S., Tarhan, L.G., O'Connell, B., Robbins, L.J., Planavsky, N.J. & Gingras, M.K. 2020: *Diopatra cuprea* worm burrow parchment: a cautionary tale of infaunal surface reactivity. *Lethaia*, Vol. 53, pp. 47–61.

Many infaunal marine invertebrates produce mucus excretions that play an important role in metal binding, authigenic mineralization and burrow stabilization. To date, only a handful of studies have characterized the functional groups that control the surface reactivity of burrow linings and backfills. This makes it difficult to place estimates on the overall impact that bioturbation has on metal cycling in tidal flats, the inner shelf, estuaries and other shallow marine environments. Here, we examined the parchment linings of *Diopatra cuprea* burrows from the Ogeechee River estuary near Savannah, Georgia, USA. Acid–base titrations coupled with Fourier transform infrared spectroscopy demonstrate that the parchment is essentially composed of hydroxyl (R-OH) groups, yielding total ligand densities of only 0.017 mmol/g. To place this value into context, it is orders of magnitude less than previously reported mucopolysaccharides for other marine worms, indicating that *D. cuprea* is essentially unreactive in the estuarine waters from which it was collected. This was corroborated by minimal Cd^{2+} adsorption to, and limited silicification of, pre-rinsed parchment. The lack of silica adsorption was surprising given that the parchment was generally coated with an abundance of quartz grains when extracted from the sediment. This suggests that perhaps the physical, rather than chemical, characteristics of the parchment material were responsible for this association. Indeed, scanning electron microscope images show that the parchment is fibrous and envelopes quartz grains, implying that detritus may get trapped by the parchment mesh. It appears that unlike many other infaunal mucopolysaccharide-rich linings that might be produced to provide reactive surfaces to which dissolved metal cations can adsorb for the organism's nutritional benefit, the parchment of *D. cuprea* may instead function to protect the animal from stresses such as predation or high-energy disturbances. □ *Chemical reactivity, Diopatra cuprea, worm parchment.*

Kurt O. Konhauser ✉ [kurtk@ualberta.ca], Weiduo Hao [whao@ualberta.ca], Yuhao Li [yuhao3@ualberta.ca], Konstantin von Gunten [vongunte@ualberta.ca], Brendan A. Bishop [babishop@ualberta.ca], Daniel S. Alessi [alessi@ualberta.ca], and Murray K. Gingras [mgingras@ualberta.ca], Department of Earth and Atmospheric Sciences, University of Alberta, Edmonton, AB T6G 2E3, Canada; Lidya G. Tarhan [lidya.tarhan@yale.edu], Leslie J. Robbins [leslie.robbins@yale.edu], and Noah J. Planavsky [noah.planavsky@yale.edu], Department of Geology & Geophysics, Yale University, New Haven, CT 06511, USA; Brennan O'Connell [oconnellb@student.unimelb.edu.au], School of Earth Sciences, University of Melbourne, Parkville, Vic. 3010, Australia; *manuscript received on 6/12/2018; manuscript accepted on 8/03/2019.*

It is widely recognized that animals play a key role in the recycling of organic carbon in marine sediments through burrowing and the concomitant mixing of fresh sediment and older sediments, grazing and mining of intact organic remains, and the ingestion of refractory organic carbon that may lead to the excretion of more labile faecal pellets. These processes become particularly relevant when one considers that, in shallow marine environments, the number of burrows present often ranges from ~100 m^{-2} for larger animals such as shrimp and lugworms to more than 50,000 m^{-2} for smaller animals such as threadworms or amphipods (e.g. Gingras *et al.* 1999). Bioturbation also influences the geochemical and mineralogical properties of sediment by increasing the transport of diagenetic reactants from seawater into the sediment where they can be adsorbed onto the mucopolysaccharides and proteins that typically line the bioturbating organisms' dwelling burrows. Similar to microbial biomass, these organic materials are studded with surface functional groups that become dominantly anionic over the pH range of marine pore waters, thus making the burrow linings highly reactive towards dissolved metal cations (e.g. Over 1990; McIlroy *et al.* 2003). Indeed, Over (1990) showed that Cu, Fe, Mn, Ni and Zn in

DOI 10.1111/let.12335

the burrow walls of *Callianassa major* were concentrated by factors between 2 and 4 times relative to the surrounding sedimentary media and that analogous Pleistocene burrow structures (i.e. *Ophiomorpha, Skolithos and Gyrolithes*) from environmentally similar strata were also enriched in metals, albeit to a lesser degree. Therefore, the reactive organic compounds produced by infauna have the potential to change the capacity of sediment to scavenge metals and pollutants, which is a less commonly discussed aspect of how animals can transform a sedimentary environment.

In experiments designed to assess the reactivity of natural burrows, Lalonde *et al.* (2010) isolated and analysed the mucopolysaccharide linings of terebellid worm burrows (*Thelepus crispus*) that are common in estuarine sediments along the Pacific coast. The authors demonstrated that mucus material possesses unusually high total ligand densities (correlating to high reactivities), on the order of 11.26 mmol/g, compared to 5.70 mmol/g for humic acids (Milne *et al.* 2001) or 3.2 mmol/g for bacterial surfaces (Borrok *et al.* 2005). This high availability of adsorptive ligands was directly translated into the quantity of metal potentially bound (e.g. using Cd) over the pH range typical of estuarine and near-shore marine settings, indicating that, on a per mass basis, worm mucus is more reactive towards dissolved metal cations than other organic compounds associated with marine sediment. That study was followed up with an assessment of the chemical properties of a commercially available purified analogue to mucopolysaccharide, mucin: the latter was used due to the inherent difficulty in isolating animal mucus from marine sediments (Petrash *et al.* 2011). Again, the mucin proved an effective biosorbent for Cd, with the concentration of reactive organic ligands in mucin exceeding 17.27 mmol/g. Given the widespread presence of mucus in burrow linings and backfills, its continuous production independent of sedimentation rates and the recognized chemical reactivity of the constituent mucopolysaccharides, Konhauser & Gingras (2011) subsequently proposed that burrow linings could represent a major pathway for sequestrating some transition metals from seawater. Given that mucus-lined burrows typically have a sharp redox interface, they not only effectively scavenge metals more efficiently than clay linings, but likely also foster the eventual geological sequestration of bioessential metals (e.g. Cd, Cu, Zn, Mo, Ni) as sulphides. Therefore, although the effects of burrow linings are not commonly discussed, their abundance and unusually high reactivity suggest that they may actually play a significant role in the global biogeochemical cycling of trace metals. However, additional work on a wider range of burrow types is needed to extrapolate initial observations on burrow mucus reactivity.

In an attempt to advance previous studies through the study of *in situ* burrows, we collected the burrow linings of *Diopatra cuprea* (Bosc 1802) from the Ogeechee River estuary, 5 km south of Savannah, Georgia, USA. *Diopatra cuprea*, also referred to as the decorator worm or ornate worm, is a species of polychaete worm commonly found in intertidal and subtidal sediments along the western Atlantic Ocean, Caribbean Sea and Gulf of Mexico. These deep-burrowing worms live within a parchment-lined tube that normally extends 20 to 30 cm below the sediment–water interface, but the tubes can extend up to a metre in length (Mangum *et al.* 1968). Two types of tube construction have been reported for *D. cuprea:* (1) an unreinforced tube which is built below the sediment–water interface as the worm moves vertically downwards and to which sand or other sediment grains adhere; and (2) a reinforced tube rising a few centimetres above the sediment–water interface (called the tube cap). The tube cap is formed when the worm extends outside its aperture and browses on the sediment to find debris (shells, pebbles, plant materials) which it drags back to the edge of its tube and cements in place as a form of armour against wave- and tide-generated currents (Myers 1972). *Diopatra cuprea* feeds at, and just above, the sediment–water interface, and its gut contents can be diverse, including diatoms, nematodes, copepods and various algae (Mangum *et al.* 1968). This suggests that *D. cuprea* actively filter feeds and may engage in interface-associated predation with both ethologies facilitated by the uniquely hooded aperture that *D. cuprea* constructs.

We were particularly interested in studying the parchment-lined tube material (hereafter, referred to as parchment) of *D. cuprea* because, at previously reported burrow densities of 20–100 m^{-2} (Myers 1972) and depths extending up to 1 m, it constitutes a significant mass of organic carbon-bearing material in an otherwise sandy environment. Further, the worms facilitate high irrigation rates, which means that large volumes of water move in and out of the tube and interact with the tube lining. The parchment has previously been characterized as a sulphated polysaccharide mucus (Myers 1972).

Geological setting

Fieldwork was conducted using a boat from the Skidaway Institute of Oceanography. The semidiurnal

tidal regime of the Ogeechee River estuary is upper micro tidal to lower mesotidal with a mean tidal range of 2.4 m, although the tidal range can reach 3.4 m during spring tides. The estuary is mixed-energy, possessing a large tidal prism and wave-generated shoals at the mouth. The estuary is oriented perpendicular to the coastline and is bordered by extensive salt marshes in its lower expanses. The Ogeechee is known as a 'blackwater' estuary because its waters are turbid due to the abundance of organic detritus and tannins derived from neighbouring marshes and forested areas.

The studied worm populations are located in the outer part of the estuary where salinities are very close to normal marine, about 30 parts per thousand (ppt). We collected parchments from two locations: Raccoon Key (A in Fig. 1; 31.840000°N, 81.050000°W) and Steamboat Pass (B in Fig. 1; 31.858860°N, 81.084274°W). At both locations, *Diopatra* parchments are exposed at low tide. Raccoon Key is a sand-dominated intertidal platform situated between the Ogeechee River and the Little Ogeechee River tidal channels. Owing to its proximity to the estuary mouth and adjacency to the main tidal channel, Raccoon Key is exposed to tide- and wave-generated currents. The sediment is dominantly upper fine-grained sand with very low silt content. Steamboat Pass is 4 km landward of Raccoon Key and is sheltered from wave energy by Raccoon Key but exposed to tidal currents. The Steamboat Pass location is a laterally accreting barrier top situated at the tidal channel margin: the intertidal sediment is lower fine-grained sand with some silt. The worm population at Steamboat Pass is found in upper very fine-grained sand with some silt.

At both locations, worm populations (based on the distribution of tube openings) range from rare and sporadically distributed (<5 m^{-2}) to very abundant (~50 m^{-2}; Fig. 2). The *Diopatra* parchment extends below depths of 40 cm and commonly reaches 2 to 8 cm above the sediment–water interface. The parchments are unornamented below the sediment–water interface and ornamented with shells, kelp and pebbles above. Parchments and associated burrows were vertically oriented (i.e. morphology referable to *Skolithos* isp.), although the part of the parchment above the sediment normally lays nearly flat on the sediment surface.

Materials and methods

Parchment collection and preparation

Unreinforced tube parchments of *D. cuprea* were collected from below the sediment surface at both field sites. Parchment samples were then immediately placed into 20-mL high-density polyethylene (HDPE) vials that were filled to the top with parchment material. The vials were filled to capacity with seawater to ensure no head space prior to sample transport. Bulk sediment samples (sediment

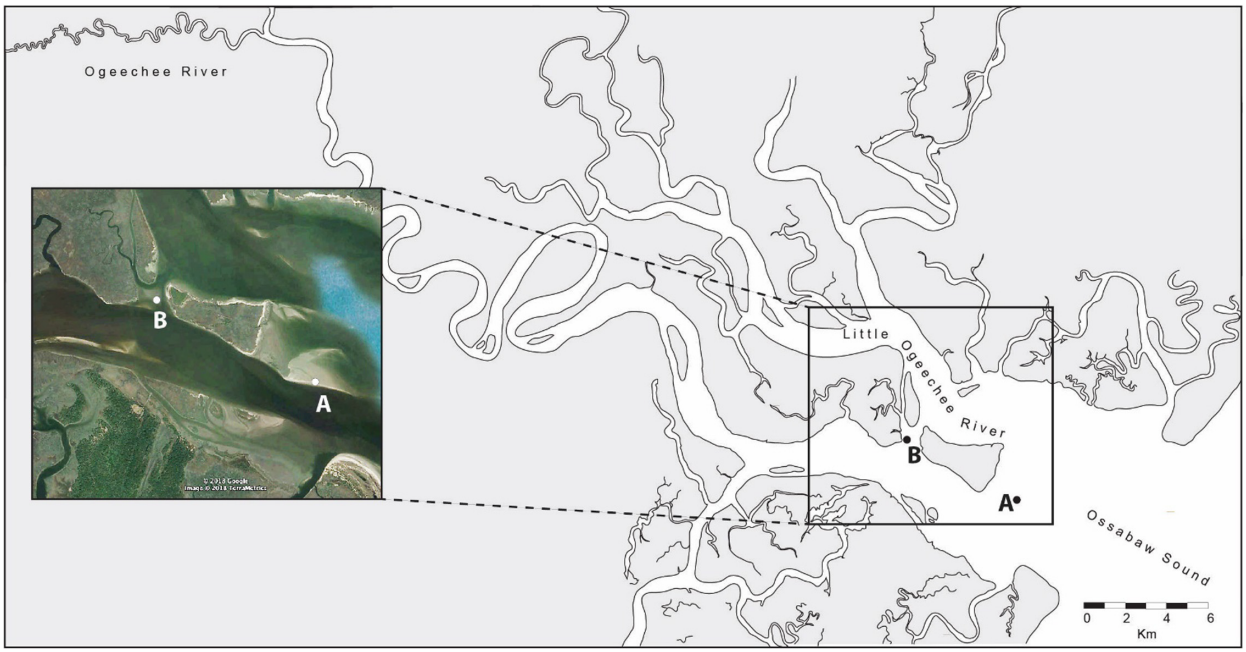

Fig. 1. Location map of the Ogeechee Estuary. A, sample location at Raccoon Key 31.840000°N, 81.050000°W. B, sample location at Steamboat Pass 31.858860°N, 81.084274°W. [Colour figure can be viewed at wileyonlinelibrary.com]

Fig. 2. Diopatra cuprea parchments exposed during low tide at Raccoon Key. Examples of tube openings are indicated with white arrows. Examples of parchment that extend above the sediment–water interface are indicated with black arrows. The straight to curved grooves are made by *D. cuprea* as they deposit feed at the sediment–water interface. Some of the grooves are modified by water from the worm's irrigation efforts and the final stages of falling tide. Scale bar is 10 cm. [Colour figure can be viewed at wileyonlinelibrary.com]

associated with but not attached to the parchment) were collected concurrently in similar HDPE vials.

Immediately upon returning to the University of Alberta (U of A), the vials with the parchment samples were prepared for the various analyses described below. First, the tubes were removed with forceps and placed in sterile petri dishes where their dimensions were measured. Although the parchment tubes can be several tens of centimetres in length while in their burrows, most unreinforced samples collected from below the surface–sediment interface tended to be on the order of 10 to 20 cm in length due to breakage during extraction. The average parchment diameter was between 0.3 and 0.5 cm (Fig. 3A).

The parchment collected from the field was heavily coated with sediment composed primarily of quartz grains (Fig. 3B). Thus, each parchment sample was rinsed with ultrapure water three times to remove loosely attached sediment on both the outside and inner lining. The amount of loosely attached sediment on parchment samples was estimated to account for ~25% of each tube sample's weight, based on a weight measurement taken before and after the initial sediment removal. After rinsing, several parchment samples were acid-washed to remove previously adsorbed metals and any sediment still attached to the parchment after rinsing. The acid wash procedure was performed by adding approximately 2.5 g of parchment to 10 mL of ultrapure water adjusted to pH 3 with hydrochloric acid (HCl) for 1 h to remove any surface-bound metals and grains. During the rinse, we did not observe any mechanical or chemical removal of the outermost organic layers of the parchment.

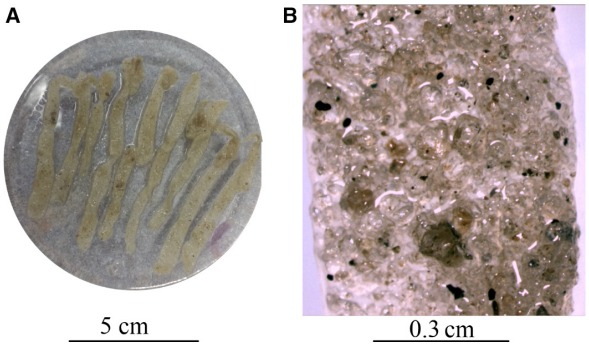

Fig. 3. A, cleaned parchment after having rinsed off the detritus. B, light microscopy image of the exterior of a piece of unrinsed parchment with abundant quartz grains. [Colour figure can be viewed at wileyonlinelibrary.com]

Analysis of liquid samples

Water samples from the field and acid leachate collected from parchment washes were analysed by inductively coupled plasma mass spectrometry (ICP-MS) on an Agilent 8800 Triple Quadrupole ICP-MS/MS at the Environmental Geochemistry Lab (U of A) using collision and reaction gases to reduce polyatomic interferences after Sakai (2015). Prior to analysis, samples were diluted in 2% nitric acid (HNO_3) and 0.5% HCl. Internal standards, measurement modes and detection limits are summarized in Table S1. The instrument was run in high matrix mode using argon (Ar) gas as the carrier and dilution gas. External calibration was done with mixtures of single-element standards (SPEX CertiPrep and Ricca Chemical) with obtained R^2 values >0.992. Internal standards, measurement modes and detection limits are summarized in Table S1.

Total digestion of bulk sediment and parchments

Bulk sediment samples were flushed with ultrapure water to remove excess salt and residual seawater. To accomplish this, 10 g of sediment was mixed with 15 mL ultrapure water, vortexed and then separated by centrifugation (15,000 g, 15 min); this procedure was repeated 3 times. Total digestion of the sediment was performed in triplicate following the method of von Gunten *et al.* (2017). Briefly, 0.1 g of sediment was pre-treated with 5 mL of 30% hydrogen peroxide (H_2O_2) and 5 mL 70% HNO_3. The remainder of each sample was then heated to 175°C and amended with 5 mL 70% HNO_3 and 5 mL 48–51% HCl. After heating to dryness, the remains were dissolved in 1 mL HNO_3 and 3 mL HCl, and the solution was

subsequently diluted to 50 mL with 2% HNO_3 and 0.5% HCl. The washed and acid-leached parchments were digested in the same way, but with 2 mL HNO_3 and 2 mL HCl following the pre-treatment.

Fourier transform infrared (FTIR) spectroscopy

Fourier transform infrared (FTIR) spectroscopy was used to determine the dominant types of organic bonds that comprise the parchment of *D. cuprea* and to assist in assigning functional group identities to the sites modelled from titration data. *Diopatra cuprea* parchment was prepared for FTIR analysis by rinsing it with ultrapure water followed by an acid wash step as described above. Samples for FTIR were then freeze-dried for 48 h prior to analysis. The freeze-dried parchment was then combined with potassium bromide (KBr) powder at a 1:150 (wt/wt) parchment:KBr ratio and hand-pressed to form a pellet. The pellet was analysed using a deuterated triglycine sulphate (DTGS) detector attached to a Thermo Nicolet FTIR Spectrometer 8700 at U of A. Infrared spectra were examined over the range of 4500–500 cm^{-1} in absorbance mode, which was then also converted into per cent transmittance. For each spectrum, 32 scans were collected with a resolution of 4.0 cm^{-1}.

Acid–base titrations

Potentiometric titrations of acid-washed parchment samples were conducted using an automated titrator (Metrohm Titrando 905) as previously described by Hao *et al.* (2018). Briefly, the pH electrode was calibrated using three commercially available pH buffers (Fisher Scientific; pH 4.0, 7.0, 10.0) before the titrations were performed. Approximately 1 g of acid-washed parchment was suspended in 50 mL of 0.56 M NaCl solution to achieve a 20 g/L suspension. The suspension and the acid and bases used for the titration process were bubbled for 30 min prior to the initiation of, and during, the titration with $N_{2(g)}$ to ensure the solutions were devoid of atmospheric $CO_{2(g)}$. Initially, a small volume of 0.1 M HCl was added to bring the solution pH to 3, followed by incremental additions of 0.1 M sodium hydroxide (NaOH) to increase the pH to 9. The volume of acid and base added, and corresponding pH changes, were determined automatically by the titration controlling software and recorded at each step of the titration. The pH was considered stable and recorded only after an electrode stability of 6 mV/min was achieved. A blank titration without parchment was also performed to ensure the proton reactivity was an inherent property of the parchment and not a function of the electrolyte solution. To ensure that the titration was reversible, and no hysteresis was induced by changes in pH (e.g. Flynn *et al.* 2017; Warchola *et al.* 2017), each analysis consisted of an up–down–up titration (between pH 3 and 9). The titration data were then used to develop a surface protonation model. In all cases, a model that employed one amphoteric surface functional group successfully simulated the parchment titration data. The surface functional group concentration and two corresponding protonation constants (pK_a values) were calculated based on the following reactions:

$$[1]\ \text{R-OH} \longleftrightarrow \text{R-O}^- + \text{H}^+$$
$$K_1 = [\text{R-O}^-] \bullet \alpha_{H+} / [\text{R-OH}]$$

$$[2]\ \text{R-OH} + \text{H}^+ \longleftrightarrow \text{R-OH}_2^+$$
$$K_2 = [\text{R-OH}_2^+] / [\text{R-OH}] \bullet \alpha_{H+}$$

where $R\text{-}O^-$, R-OH and $R\text{-}OH_2^+$ denote the negatively, neutral and positively charged protonation states of the one type of surface functional group, respectively; α_{H+} represents the activity of protons; and the square brackets indicate concentrations of surface sites at the three protonation states.

Previous confocal microscopy studies by Phillips & Lovell (1999) have demonstrated that parchments of *D. cuprea* support biofilms with an average thickness of only 60 μm and contain abundant bacteria occurring as single cells and in micro-colonies. We were not concerned with confounding the reactivity of the biofilms with the parchment itself because: (1) we did not fix these tubes in preservative to maintain intact microbial biomass; (2) the biofilm layer is thin (micrometres) compared to the parchment lining (millimetres); and (3) before the titrations, we cut the parchment longitudinally and washed both the outside and inside with ultrapure water to remove loosely attached sediment and likely the majority of the associated biofilm.

Cadmium adsorption experiments

Adsorption experiments onto acid-washed parchment samples were performed to quantify the metal-binding capacity of the surface ligands. Cadmium was specifically chosen in our study versus other metal cations for the following reasons: (1) it remains largely soluble at seawater pH; (2) its use in laboratory settings is not complicated by the precipitation of cadmium carbonate or hydroxide solids at our experimental conditions; (3) to facilitate comparison with other metal adsorption studies involving humic acids, bacterial species or clay minerals where Cd is the typically chosen metal (e.g. Yee & Fein 2001;

Alessi & Fein 2010; Lalonde *et al.* 2010; Petrash *et al.* 2011; Liu *et al.* 2018); and (4) for environmental relevance to estuaries and other near-shore waters where Cd concentrations may be elevated (Petersen *et al.* 1998).

Approximately 0.2 g of parchment sample was suspended in 20 mL of 0.56 M NaCl to make a 10 g/L suspension. For the adsorption experiments, a 1 ppm Cd solution was prepared by serially diluting a commercially available, certified 1000 ppm Cd standard (Fisher Scientific) with ultrapure water. Batch experiments were performed over a pH range of 6 to 9 in steps of 1 pH unit. The pH of each sample was adjusted by adding small aliquots of 0.01 M NaOH or HCl solutions as required, and this process was repeated three times until a stable pH was achieved. All adsorption experiments were performed in duplicate at room temperature and equilibrated over a period of 60 h.

Aliquots of ~0.5 mL were removed by syringe and passed through a 0.22-μm nylon membrane filter. A Cd adsorption blank was not run simultaneously, but previous experiments run under similar conditions showed negligible Cd adsorption (Hao *et al.* 2018). Furthermore, chemical equilibrium modelling of Cd speciation of experimental solutions was performed with the HYDRA and MEDUSA software package (Puigdomenech 2006) with the default activity corrections and stability constants, which include complexes with Cl^- at seawater conditions. The models indicate negligible Cd precipitation for the given experimental conditions.

Silicification experiments

To explore the potential sorption of negatively charged aqueous complexes, the reactivity of parchment samples towards chemically reactive silica was examined. Specifically, our aim was to test whether the parchment was susceptible to silicification in a manner akin to other biological surfaces. To assess the silicification potential, parchment samples were first rinsed three times in ultrapure water in order to remove as many residual sand grains as possible without damaging the structural integrity of the parchment. Parchment samples for silicification tests were not acid-treated as described in other analytical steps above. All glassware used in the silicification experiments was acid-washed for a minimum of 24 h, rinsed three times with ultrapure water and allowed to air dry while inverted.

Initially, ~5 mL of a 2000 ppm SiO_2 solution prepared using sodium meta-silicate nonahydrate ($Na_2SiO_3 \bullet 9H_2O$) was added gravimetrically to ~45 mL of 0.56 M NaCl solution buffered at pH 8 with 0.1 M H_3BO_3. This resulted in each silicification sample having an initial SiO_2 concentration of ~400 ppm. Approximately 1 mL was removed from each sample to verify the initial SiO_2 concentration by ICP-MS/MS on an Agilent 8800 as described above. Following the addition of the silica solution, each sample was adjusted to pH 8.1 $\pm$ 0.1 by addition of small aliquots of 12.1 M HCl. A 0.4 g sample of washed *D. cuprea* parchment was then added to the silica solution, allowed to equilibrate with the silica-rich solution for 24 or 48 h, and then fixed in a 2% paraformaldehyde and 2.5% glutaraldehyde-buffered fixative solution prior to SEM imaging. A sample of the solution was taken at 24 and 48 h to determine the final concentration and corresponding decrease in SiO_2 over the course of the experiment and analysed by ICP-MS/MS.

Alongside the silicification samples, two control cases were considered: (1) an admixture of the SiO_2 solution and buffered NaCl solution to determine the extent of inorganic SiO_2 precipitation in the absence of parchment and (2) a parchment sample in NaCl solution with no added SiO_2.

Scanning electron microscopy (SEM)

An unrinsed parchment sample, clean parchment sample (rinsed by ultrapure water and acid) and detached sediment sample from the parchment were prepared for SEM imaging. *Diopatra cuprea* samples for SEM were stored in a 2% paraformaldehyde and 2.5% glutaraldehyde-buffered fixative solution after samples were received, while the silicified samples were fixed immediately following the silicification experiments. Samples remained in fixative solution overnight and were then washed with a 0.1 M phosphate buffer solution for 10 min. The phosphate buffer wash was repeated in triplicate, after which samples were dehydrated through a graded ethanol series. The ethanol series consisted of 50%, 70%, 90% and 100% solutions (v/v), with a 20-min incubation time at each stage. Samples were further processed in a series of ethanol and hexamethyldisilazane (HMDS) solutions with similar incubation times. Finally, parchment samples were left in a 100% HMDS solution for 16 h to ensure complete dehydration.

The sediment samples were directly transferred onto a SEM stub and placed in a fume hood for an additional 16 h to air dry. All samples were sputter-coated with carbon and imaged on a Zeiss Sigma 300 VP-FESEM at 10 kV. Elemental characterization of the parchment samples was examined on a Bruker energy-dispersive X-ray spectroscopy (EDS) system directly connected to a Zeiss Sigma 300 VP-FESEM.

Results

Water, bulk sediment and parchment composition

Major elements quantified by ICP-MS/MS (Table 1) from water samples were Na, Mg, S, Ca and K with up to 11.9%, 1.1%, 0.8%, 0.4% and 0.3%, respectively. All water samples had a circum-neutral pH.

The parchment material has similar metal concentrations as the bulk sediment (Table 2), likely due to the sand particles which were strongly attached to it even after rinsing. This is consistent with the sand on the parchment representing a major contributor to the sample weight (i.e. 25 wt%). However, when compared against each other (Fig. 4), differences between the bulk sediment and the parchment material may be observed. The parchment contains more than triple the Mg, more than double the S, and more than quadruple the P. The latter two elements are likely attributable to the organic material comprising the parchment, whereas Mg is likely adsorbed, as is suggested by the metal concentration in the leachates (Table 1).

Table 1. Analysis results for the water samples and the 2 acid leaches collected after washing of parchment.

	Units	Steamboat Pass	Raccoon Key	Acid leachate 1	Acid leachate 2
pH		7.06	7.39		
Major elements					
B	ppm	3.59	4.46	0.80	0.86
Na	ppm	17577.85	11881.75	779.54	807.66
Mg	ppm	803.97	1077.99	22.22	23.77
Si	ppm	6.06	2.78	1.22	1.46
K	ppm	280.04	276.96	7.51	8.45
S	ppm	613.08	682.03	14.02	11.54
Ca	ppm	353.26	391.01	13.07	13.33
Sr	ppm	5.27	5.35	0.19	0.18
Minor elements					
Li	ppb	120.61	140.69	4.31	4.10
Al	ppb	88.80	128.03	4.27	4.61
P	ppb	94.46	36.51	289.46	270.80
V	ppb	3.27	2.59	5.04	4.94
Cr	ppb	8.70	13.82	0.82	1.02
Mn	ppb	8.19	4.21	43.40	24.09
Fe	ppb	53.41	22.00	12.80	7.54
Co	ppb	0.11	0.17	0.11	0.07
Ni	ppb	0.74	4.11	3.32	2.69
Cu	ppb	25.01	36.75	2.12	1.24
Zn	ppb	22.24	43.98	21.09	4.53
As	ppb	2.42	2.36	3.26	3.25
Mo	ppb	7.88	9.92	0.63	0.49
Se	ppb	2.57	2.89	0.63	0.46
Cd	ppb	0.07	<0.02	<0.02	<0.02
Ba	ppb	19.50	17.98	1.06	1.02
Ce	ppb	0.06	0.07	0.06	0.03
Pb	ppb	20.50	29.84	0.07	0.15
Th	ppb	0.01	0.02	0.01	0.01
U	ppb	2.23	2.65	<0.005	<0.005

The acid leaches of the parchment materials conducted at pH 3 contain metals that were weakly sorbed to the surface. The leachate mostly contains Na and Mg, with up to 808 ppm and 24 ppm,

Table 2. Elemental concentrations in the matrix sand and the parchment.

	Total digestion (Avg ± Std, $n = 3$)	
	Bulk sediments	Parchment
Li	4.47 ± 1.71	3.67 ± 0.26
B	11.21 ± 3.17	1.94 ± 0.73
Na	926.90 ± 86.16	919.19 ± 145.46
Mg	252.29 ± 60.03	850.99 ± 52.23
Al	3715.19 ± 619.65	3733.91 ± 671.62
K	1913.75 ± 165.24	1811.74 ± 382.85
P	610.84 ± 274.28	1734.11 ± 114.62
S	125.56 ± 37.97	517.56 ± 99.32
Ca	2867.49 ± 1287.71	3625.75 ± 792.74
V	4.61 ± 3.50	4.36 ± 0.86
Cr	5.37 ± 4.72	3.94 ± 0.83
Mn	51.28 ± 45.57	72.10 ± 13.14
Fe	2334.70 ± 1476.96	2721.85 ± 291.50
Co	0.35 ± 0.19	0.40 ± 0.04
Ni	0.49 ± 0.13	0.56 ± 0.08
Cu	<0.035	<0.035
Zn	2.33 ± 1.21	0.19 ± 0.26
Sr	27.39 ± 9.53	33.90 ± 4.47
As	0.78 ± 0.27	0.98 ± 0.05
Se	<0.06	<0.06
Mo	0.15 ± 0.05	0.15 ± 0.02
Cd	0.06 ± 0.04	0.07 ± 0.02
Ba	66.28 ± 11.44	58.19 ± 14.23
Ce	12.27 ± 8.03	18.92 ± 2.40
Pb	4.57 ± 3.11	0.81 ± 0.58
Th	1.58 ± 1.31	2.85 ± 0.52
U	0.67 ± 0.46	0.84 ± 0.30

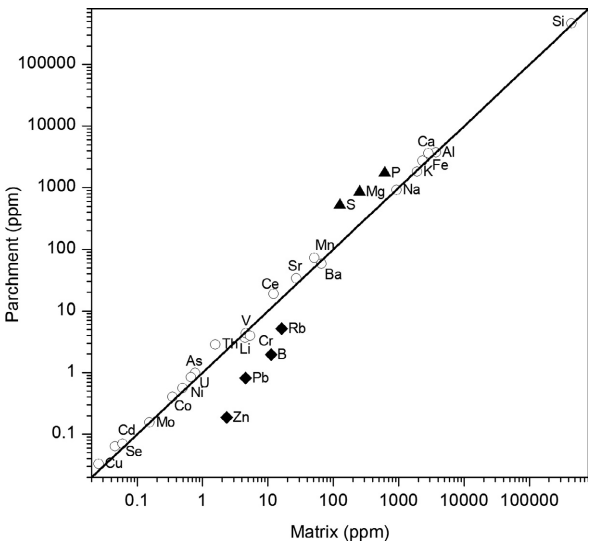

Fig. 4. Concentrations of elements in the matrix sand versus the acid-leached parchment. The straight line represents a 1:1 correlation. Elements above the line are shown as filled triangles (▲), while elements below are shown as filled diamonds (◆).

respectively (Table 1). Other important constituents with concentrations below 20 ppm are S, Ca, K, Si, B, P and Sr.

Fourier transform infrared (FTIR) spectroscopy

The FTIR data for the *D. cuprea* parchment are shown in Figure 5. A number of vibrational bands are observed, each of which corresponds to an organic bond within the parchment. The wide absorption band at 3430 cm^{-1} is consistent with the stretching of O-H hydroxyl groups, whereas the strong peak at 1080 cm^{-1} is indicative of C-O and C-O-C stretching (Coates 2000; Naumann 2000) and likely represents polysaccharides (Yee *et al.* 2004). The two smaller peaks in the region of 2800–3000 cm^{-1} are indicative of C-H stretching of $>CH_2$ and CH_3 functional groups, which can be attributed to fatty acids from membrane phospholipids (Yee *et al.* 2004). Absorption bands between 1800 and 1500 cm^{-1} are suggestive of amide I and II bands (Naumann 2000; Yee *et al.* 2004), and the band of small amplitude around 1250 cm^{-1} could be due to P=O stretching of PO_2^- phosphodiesters (Naumann 2000).

The FTIR spectra from the parchment differ significantly from those of the mucus lining of the terebellid burrows, as determined by Lalonde *et al.* (2010). Overall, the parchment shows a suppressed FTIR signal, especially in terms of the amide I and II bands and the OH binding; however, there is an enhanced C-O stretch characteristic of polysaccharides that dominates the parchment materials. Furthermore, the infrared data show that the parchment is lacking phosphoryl and sulphhydryl functional groups, both of which are present in the mucus previously studied by Lalonde *et al.* (2010).

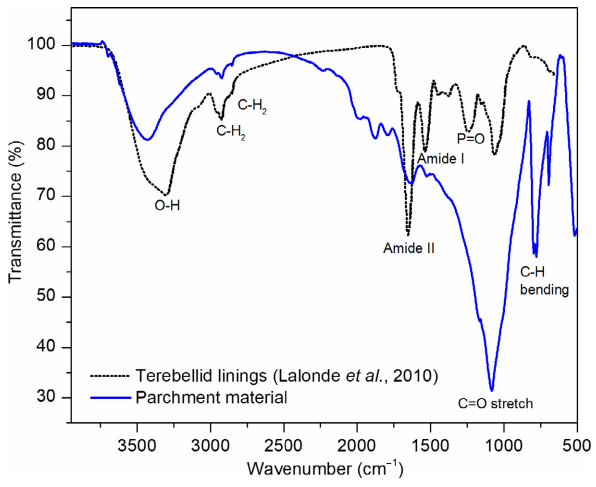

Fig. 5. Fourier transform infrared (FTIR) spectroscopy of parchment material (blue line). As a comparison, the terebellid linings analysed by Lalonde *et al.* (2010) are shown in black. [Colour figure can be viewed at wileyonlinelibrary.com]

Acid–base titrations

The titration curves for the parchment and a blank titration are provided in Figure 6. They show that the parchment is highly protonated across the pH range studied. The protonation model results are summarized in Table 3. Briefly, the surface is best modelled as a single, amphoteric functional group with a site concentration of $1.17 \pm 0.15 \times 10^{-5}$ mol/g, and logK values of 8.29 and −8.95 for the protonation (reaction 1) and deprotonation reactions (reaction 2), respectively. Models invoking two- or three proton-active sites were attempted, but the one-site model provided the best fit to the potentiometric titration data, as determined by the variance, V(Y), value in the modelling software program FITEQL 4.0 (Herbelin & Westall 1999).

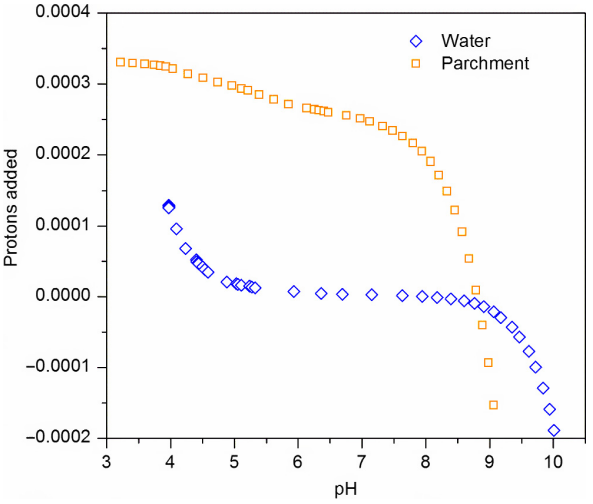

Fig. 6. Potentiometric titrations of parchment and a blank. Orange squares represent parchment titration data (i.e. the protons added during titration process and the corresponding pH change), and blue diamonds represent pure water titration data (the blank). For the *y*-axis, 'protons added' refers to the net proton budget during the titration process, which is represented by the difference between molar concentration of acid and base added into the titration system. [Colour figure can be viewed at wileyonlinelibrary.com]

Table 3. Summary of protonation model results.

	Site concentration (mol/g)	Log K1	Log K2
Parchment 1	1.26×10^{-5}	−8.90	8.55
Parchment 2	1.00×10^{-5}	−8.76	8.22
Parchment 3	1.26×10^{-5}	−9.18	8.10
Average	$1.17 \pm 0.15 \times 10^{-5}$	−8.95 ± 0.21	8.29 ± 0.23

Figure 7 shows how the speciation of the surface functional group changes with solution pH. At pH < 7.5, surface groups are highly protonated ($R\text{-}OH_2^+$) and, as pH increases above 7.5, the surface begins to deprotonate as the concentration of $R\text{-}OH_2^+$ decreases. This is accompanied by a concomitant increase in the concentration of deprotonated sites ($R\text{-}O^-$). At pH 8.62, the concentrations of $R\text{-}O^-$ and $R\text{-}OH_2^+$ are equal, and the surface proton charge is zero, representing the parchment's point of zero net proton charge (PZNPC). Thus, at pH < 8.62, *D. cuprea* parchments have a net positive surface charge, while at pH > 8.62, the parchment has a net negative surface charge. The FTIR data are consistent with the modelled surface ligand being a hydroxyl group, as hydroxyl groups typically deprotonate at alkaline pH conditions. Compared to the mucus samples of Lalonde *et al.* (2010), functional group site concentrations for the parchment of *D. cuprea* are two orders of magnitude lower. This could be due to the mucus samples being purely organic, whereas the parchment is an admixture of organic matter and quartz sand, with the latter having low ligand densities on the order of 10×10^{-5} mol/m^2 (e.g. Sverjensky & Sahai 1996).

Cd adsorption experiments

Figure 8 shows that, under our experimental conditions, Cd is mainly complexed with Cl^- across the examined pH range (6 to 9). Three aqueous complexes with chloride exist at our experimental conditions: $CdCl_2^0$, $CdCl^+$ and $CdCl_3^-$. With increasing pH, aqueous Cd hydroxide complexes are expected to form, and at pH above 11, $Cd(OH)_{2(s)}$ is indicated to precipitate. At the conditions under which our metal adsorption experiments were run, no Cd precipitation is indicated by the geochemical modelling, consistent with previous work (Lalonde *et al.* 2010; Hao *et al.* 2018). Accordingly, all Cd losses observed are attributed to the adsorption of Cd to the parchment surface.

Figure 9 displays the amount of Cd adsorbed onto the parchment surface as a function of pH. As indicated, the amount of Cd adsorbed onto parchment at pH 6 is around 25%, with a minor increase to 30% at pH 7.5. By pH 8.7, the proportion of Cd adsorption

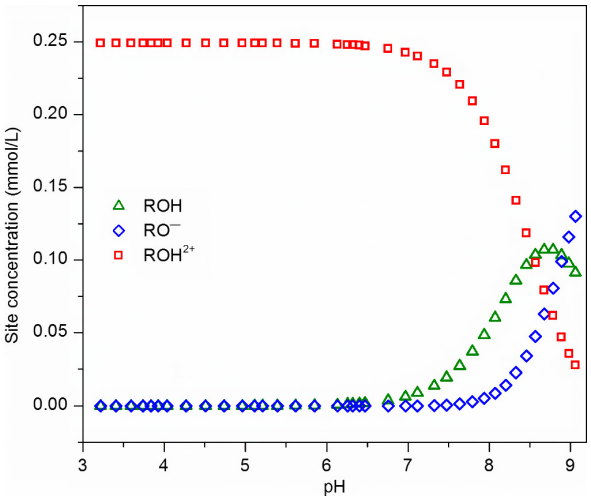

Fig. 7. Speciation diagram of surface functional groups. Blue diamonds represent changes in surface $R\text{-}O^-$ group concentration with solution pH; red squares represent changes in surface $R\text{-}OH_2^+$ group concentration with solution pH; and green triangles represent changes in R-OH concentration with solution pH. [Colour figure can be viewed at wileyonlinelibrary.com]

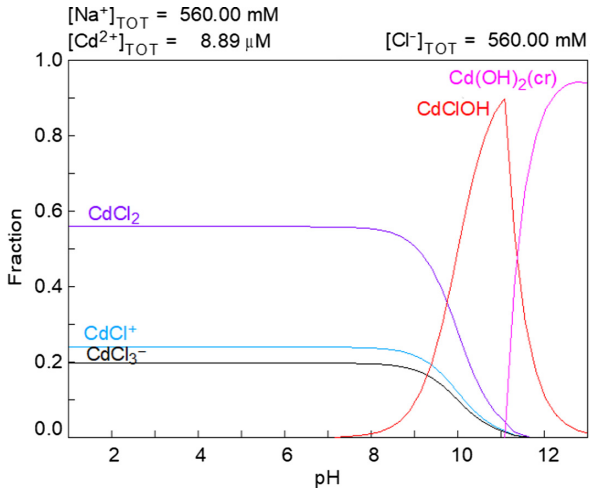

Fig. 8. Speciation diagram for Cd under the experimental conditions demonstrating that the metal exists as a chlorinated compound in seawater, and not as the free metal cation, Cd^{2+}. [Colour figure can be viewed at wileyonlinelibrary.com]

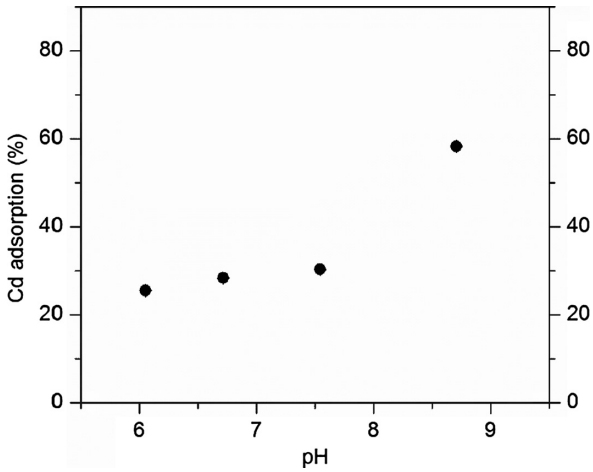

Fig. 9. Cd adsorption as a function of solution pH. The initial Cd concentration is 1 ppm; parchment suspension is 20 g/L. Data are represented as the per cent of Cd removed by parchment.

increases to almost 60%. This is consistent with both the titration and Cd speciation results. Our modelling of titration data shows that, at pH conditions below 8, the parchment surface functional group is dominated by the doubly protonated surface species ($R\text{-}OH_2^+$). These ligands can attract negatively charged Cd species such as $CdCl_3^-$, which comprises approximately 20% of the total dissolved Cd(II) at pH 8 (Fig. 8). With increasing pH, the surface functional group is increasingly deprotonated and exhibits increasing affinity for positively charged species such as $CdCl^+$, so that at pH ~8.7, both cationic and anionic species of Cd can be adsorbed onto the parchment surface. Although 60% of the Cd is adsorbed onto the parchment surface, the Cd sequestration capacity of our parchment is lower compared to previous studies that have higher functional group concentrations (Lalonde *et al.* 2010; Petrash *et al.* 2011). For instance, our parchment has 0.03 mg/g Cd bound to its surface at pH 7.5, as compared to higher values for the mucus of *T. crispus* (~2.25 mg/g; Lalonde *et al.* 2010) and commercially available mucin (~3.43 mg/g; Petrash *et al.* 2011).

Silicification of the parchment

Based on the ICP-MS/MS data, minimal silica was removed from solution by the parchment following either the 24- or 48-h treatments. The majority of silica removal was due to inorganic precipitation as evidenced by similar removal amounts in the abiogenic silica control and samples where parchment was included. Thus, it is unlikely that the parchment contributed to appreciable removal of silica from the solution. This is corroborated by SEM imaging of parchment before, and after, the silicification experiment. There are no amorphous silica particles observed on samples that were placed in silica solutions for either 24 h or 48 h. EDS analysis of both sample parchment and control parchment shows no distinct increase of Si in their elemental compositions as mass percentage (Fig. 10), which again indicates that little silica adsorbed onto the parchment surface when exposed to supersaturated silica solutions.

Scanning electron microscopy

SEM imaging of unrinsed reinforced parchment reveals a strong bonding between the exterior surface of the parchment and quartz grains (Fig. 11A), the latter being subangular to subrounded, well sorted, very fine-grained sand. The inside of the parchment, however, appears to be completely free of quartz grains (Fig. 11B). The fibrous structures of the parchment intertwine with each other, resulting in pores that are only 20 to 200 μm in diameter. Perhaps beneficially, the quartz encrustation of the outer parchment and small pores throughout the

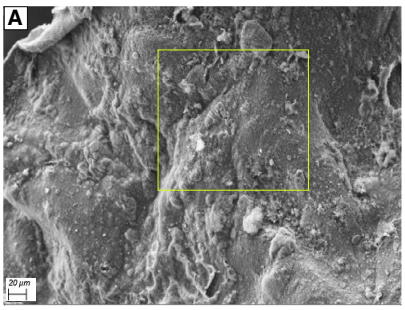

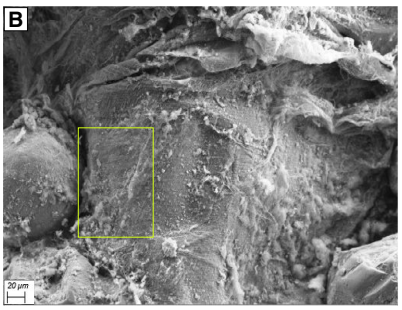

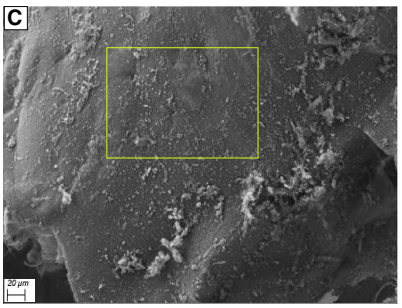

	O	Si	P	Ca
A	36.02	3.61	6.95	2.30
B	35.04	3.28	7.43	3.80
C	40.07	2.89	4.98	1.02

Fig. 10. SEM micrographs of parchment samples after silicification. A, parchment sample after 24 h in supersaturated silica solution. B, parchment sample after 48 h in supersaturated silica solution. C, parchment sample after 24 h in NaCl solution without added silica. EDS analyses of each sample are listed in the table in mass percentage for element O, Si, P and Ca. Area examined in each sample is highlighted in yellow rectangle. [Colour figure can be viewed at wileyonlinelibrary.com]

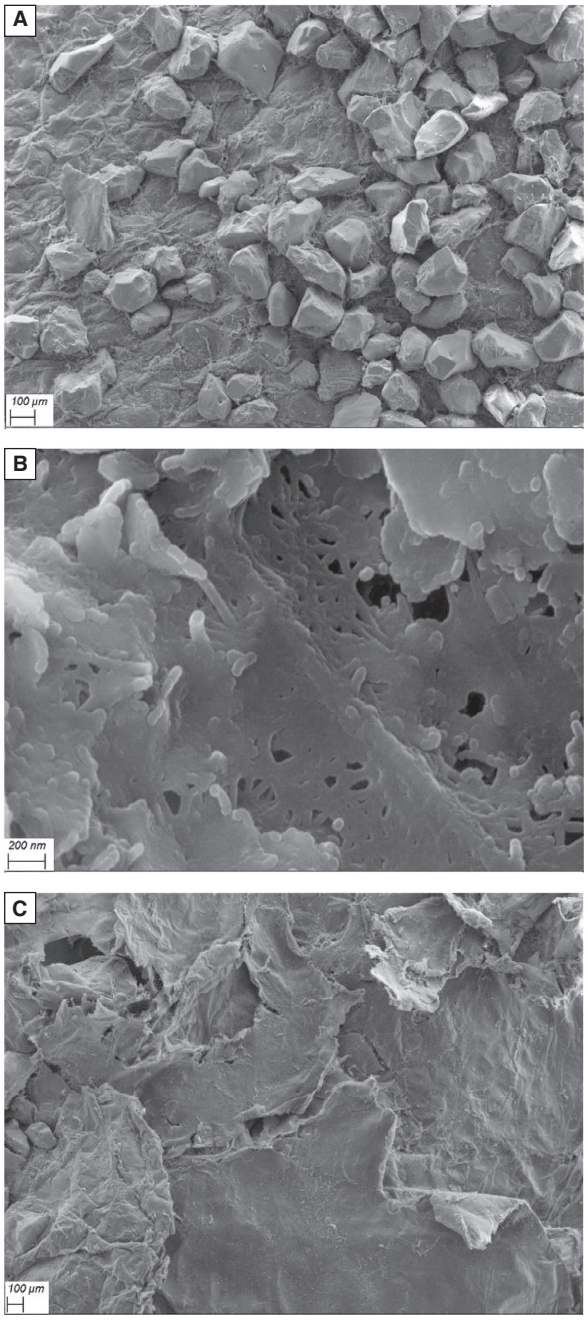

Fig. 11. SEM micrographs of parchment material. A, exterior of an unrinsed sample with quartz grains firmly attached. B, interior of an unrinsed sample showing the fibrous nature of the parchment material. C, exterior of rinsed parchment showing the fine layering of the material and the paucity of sediment grains.

parchment contribute to the low porosity and permeability of the parchment, which protect *D. cuprea* from strong currents, while still permitting water to pass through the parchment to provide the inhabitant with sufficient nutrients. The exterior of the rinsed samples is similar to the inner lining of the unrinsed ones (Fig. 11C). At a higher magnification, it becomes evident that parchment is made of multiple layers of woven strands, with common diatoms and trace amounts of clay minerals.

Discussion

When the parchment samples were collected, it was our anticipation that the organic material would have electronegative surface properties similar to the worm mucus previously described in the literature. For the burrowing terebellid worms (*T. crispus*) studied by Lalonde *et al.* (2010), acid–base titrations revealed that the mucous material possesses unusually high proton reactivity, corresponding to high ligand concentrations of 11.26 ± 1.79 mmol/g summed over pH 4 to 10, with proton-exchanging ligands distributed approximately equally across the titration range (Lalonde *et al.* 2010). Discrete ligand modelling indicated that three ligands of *T. crispus* were sufficient to accurately describe proton adsorption across the titration range. When considered in combination with FTIR and compositional data (i.e. proteins, carbohydrates and lipids in an approximate ratio of 200:50:1), the modelling also indicated the presence of abundant proton-exchanging carboxyl, phosphoryl and sulfhydryl functional groups (reactions 3–5).

[3] $R\text{-}COOH + OH^- \rightarrow R\text{-}COO^- + H_2O$

[4] $R\text{-}PO_4H_2 + OH^- \rightarrow R\text{-}PO_4H^- + H_2O$

[5] $R\text{-}SH + OH^- \rightarrow R\text{-}S^- + H_2O$

When the commercial analogue to natural mucus – partially purified Type III porcine gastric mucin – was similarly analysed by Petrash *et al.* (2011), it was shown that it mimicked the acid–base and metal complexation behaviour of the mucus excreted by terebellid polychaete worms, but it was slightly more reactive over the same experimental pH range; total functional group concentrations available for metal binding were 17.27 ± 1.05 mmol/g. At marine pH, nearly two-thirds of the total ligands in mucin-type material were deprotonated and thus available to participate in metal cation adsorption reactions.

In both previous adsorption studies using Cd^{2+} (Lalonde *et al.* 2010; Petrash *et al.* 2011), it became evident that the mucins served as efficient sorbents for the metal, potentially due, in part, to high sulfhydryl functional group content that strongly binds chalcophilic elements such as Cd (reaction 6). Despite being quantitatively less abundant that the carboxyl and phosphoryl groups (~15% of the sites in terms of mmol/g; Lalonde *et al.* 2010), thiols (organosulphur compounds containing a carbon-

bonded sulfhydryl group) have previously been shown to have the highest metal adsorption affinity (e.g. Mishra *et al.* 2010; Yu *et al.* 2014; Nell & Fein 2017):

[6] $R\text{-}SH + Cd^{2+} \leftrightarrow R\text{-}SCd^{+} + H^{+}$

The Ogeechee River *D. cuprea* parchment contains only one major functional group, and it has a higher pK_a value than the waters in the Ogeechee River estuary (pH 7.06 at Little Ogeechee and 7.39 at Raccoon Key). In the light of the FTIR data, those ligands most likely are hydroxyl (R-OH) groups (reaction 7):

[7] $R\text{-}OH + OH^{-} \rightarrow R\text{-}O^{-} + H_2O$

Interestingly, the parchment does not appear to contain carboxyl, phosphoryl and sulfhydryl functional groups that are present in the terebellid worm mucus (e.g. Lalonde *et al.* 2010). Moreover, when the overall ligand densities are compared between parchment (0.017 mmol/g) and *T. crispus* mucus (11.26 mmol/g), the former is essentially unreactive in the estuarine waters from which it was collected and therefore has much lower reactivity towards trace metals. This is corroborated not only by the lesser amount of Cd bound to the parchment as compared to mucus, but also by the paucity of metals released from the parchment during the acid leaches (Table 2), confirming that, aside from attached halite (NaCl) and quartz, the parchment contains comparatively low concentrations of metals.

The enrichment in R-OH groups in the parchment is broadly similar to the surface properties of sheaths, the outermost extracellular material that a number of filamentous iron- and manganese-depositing bacteria, as well as cyanobacteria, produce. Their structure resembles a hollow cylinder when devoid of cells, and they are often composed of neutral sugars, along with variable quantities of uronic and amino acids (e.g. Weckesser *et al.* 1988; Phoenix *et al.* 2002). One common feature seems to exist among the broad group of ensheathed microorganisms, that is, their sheaths have minute particle spacing that makes them impervious to large molecules. It is thus likely that they serve as an additional permeable layer or chemical sieve that filters out harmful macromolecules (e.g. Phoenix *et al.* 2000). Moreover, the sheath material in cyanobacteria has a different surface charge from that of the underlying wall material, implying that the sheath may mask the charge characteristics of the wall, possibly by exposing hydrophobic or uncharged surfaces to the external milieu (Phoenix *et al.* 2002). For cyanobacteria growing on siliceous sinters at hot springs, as an example, this property facilitates hydrogen bonding between the hydroxy groups associated with the sugars and the hydroxyl ions of the silica. The proposed benefit to the cells is that not only can they adhere to the submerged silica substratum and not be washed away by the effluent, but the sheath serves as a physical filter that restricts silica to its outer surface. The suggestion that an enclosing sheath of low electronegativity is important in inducing hydrophobicity (and thus encouraging surface adhesion) is corroborated by observations that the free-swimming hormogonia produced by benthic cyanobacteria are all hydrophilic in nature (Fattom & Shilo 1984). These pelagic, transient phases lack an extracellular sheath, thus exposing the highly electronegative cell wall, which, in turn, may contribute significantly to the hormogonia's hydrophilic characteristic.

Given that parchment is enriched in R-OH groups, one might expect that it would react to solid phase and dissolved silica in a similar manner to cyanobacterial sheaths. On the one hand, the silicification experiments demonstrated that the parchment material does not adsorb silica or facilitate amorphous silica precipitation. This is somewhat surprising given that dissolved silica polymers (as would be expected at supersaturation) have a net negative charge, owing to their low point of zero charge – averaging pH 1.8 (Parks 1965), and that the parchment is dominated by $R\text{-}OH_2^{+}$ groups at the estuarine pH. However, the parchment does not have significant proton reactivity, that is the site concentrations are quite low compared to worm mucus (e.g. Lalonde *et al.* 2010). Therefore, the most parsimonious explanation might be the sites on the parchment are reactive towards Si, similar to any other –OH groups, but they are of relatively low abundance, so we did not observe a measurable change in Si solution concentration during the silicification experiments. It is also important to note that the raw parchment was heavily coated in quartz grains when removed from the sediment, suggesting that if the parchment material was not chemically reactive to quartz (with a zero point of charge of 2.2; Parks 1965) then perhaps the physical, rather than chemical, characteristics of the parchment material were responsible for this association. For instance, the SEM images show that the parchment is fibrous, suggesting that grains may get trapped by the parchment mesh. Optical images also show that the grains are partially enveloped by the parchment and, like the shell, kelp and pebble clasts affixed within the aperture, quartz is more likely included in the parchment as opposed to adhered to the exterior of the parchment.

An important implication from this study is that the low reactivity towards Si and other metals indicates that mucus-lined burrows need not leave a

trace in the geological record. In other words, while some trace fossils impart a distinct geochemical and petrographic signature because of the reactivity of their organic linings, the lack of reactivity towards silica and trace metals exhibited by *D. cuprea* indicates that some trace fossils may be indistinguishable from the surrounding host rock. At this present time, we do not know whether the properties of *D. cuprea* parchment are an exception or whether it may be common among other burrowing animals. That being the case, it is our opinion that determining the prevalence of burrows with organic linings is as essential as determining bioturbational intensity when trying to reconstruct how infaunalization transformed the Earth system. Owing to the potential for burrow linings to concentrate organic matter and clay minerals, fossilized burrows have commonly been viewed as potential initiation points for sediment diagenesis. Indeed, the diagenetic classification of trace fossils (e.g. reflecting the presence or absence of localized cementation of tube linings or burrows, nodules developed from burrow-localized dissolution, and diagenetic haloes) (Abdel-Fattah *et al.* 2011) reflects the impact ichnofossils have, as compositional anisotropies, on diagenesis in marine sediments. Importantly, cement distributions associated with trace fossils play a major role in their passage to the fossil record and their subsequent recognition as ichnofossils. However, trace fossils lacking reactive burrow linings will not be readily recognizable, except where the enclosing lithology (and burrow infill) is heterogeneous. Moreover, the unreactive character of the parchment of *D. cuprea* suggests that a lack of ichnofossil-associated trace metal enrichments does not necessarily indicate the lack of a burrow lining. Given that whether a burrow is lined or unlined will substantially impact not only local redox gradients but also rates of advection of seawater into the surrounding sediments (cf. Aller 1983), our ability to recognize ancient burrow linings is critical to reconstructing the diagenetic impact of ancient infaunalization. This work thus highlights the caution that should be taken in assuming that all ancient traces induced significant sedimentary oxidation, rather than fostering sharp redox interfaces.

The compositional differences between *D. cuprea* parchment and *T. crispus* mucus lead to the conclusion that the organic materials produced by these vermiform infauna serve different purposes. It has previously been speculated that mucus might be produced to provide a reactive surface to which dissolved metal cations can adsorb, in essence acting as a nutrient sieve that concentrates metals and nutrients for the organism's benefit, or perhaps the benefit of the microbial colonies that typically accompany the linings of burrowing organisms in a symbiotic fashion (Lalonde *et al.* 2010). Notably, several trace fossil forms have been considered as likely platforms for chemo-symbiosis with microbes, including the iteratively branched *Chondrites* isp. (Seilacher 2007) and farming traces that include the broader group of trace fossils known as graphoglyptids (Seilacher 2007). One cannot discount that in other types of trace fossils, such as the pellet-lined shrimp burrow *Ophiomorpha isp*. or the heavily sediment-lined worm burrow *Rosselia isp*., metal enrichment (e.g. iron) contributes to an inchoate oxide cement that serves to bolster the structural integrity of the lining. In short, the concentration of metal cations in linings of burrows certainly may have both metabolic and structural advantages.

It is interesting that most animals with pronounced tubes that are composed of mucus secretions rather than sediment are, in fact, made by animals dominantly engaged in filter feeding or interface-associated deposit feeding. Just a few examples include *Diopatra* sp., maldaniid polychaetes (Zorn *et al.* 2010) and serpulid polychaetes (Vinn 2013). In all of these examples, the animal derives nutrition from the sediment–water interface or the water column and a chemo-symbiotic relationship is therefore not needed to obtain nutrition. Also, the tube is sufficiently strong to protect the animals from stresses such as animal predation or high-energy disturbances. It may be that mineral precipitation on linings such as those of *D. cuprea* would have a negative effect on the permeability of the burrow lining and would, if present, effectively limit the transport of solutes into and out of the animal's living space, hindering burrow irrigation (cf. Aller 1983) and limiting the inhabitant's ability to draw other nutrients from the sediment.

Conclusions

Invertebrate burrow linings have been identified as an important sink for cations, and as such, they provide a mechanism for enriching marine sediments in certain elements. Along with potentially facilitating some aspect of the tracemaker's infaunal lifestyle, such as expanding food resources or structural enhancement of the living space, localized enrichment of various elements introduces compositional heterogeneities in associated strata that influence later eogenetic and diagenetic reactions and potentially play some role in the preservation of the trace fossil. The parchment linings of *Diopatra cuprea* enigmatically show very little reactivity. We speculate

that the tube is strictly used as a physical barrier and that the lack of burrow reactivity may serve to preserve the lining's permeability for irrigation of the worm's living space. Importantly, burrows characterized by such linings do not present compositional heterogeneities that will focus later diagenetic reactions. Rather, the burrow can only be preserved as a textural (grain-size) heterogeneity.

Acknowledgements. – The research presented in this manuscript was funded by Natural Sciences and Engineering Research Council of Canada (NSERC) to Kurt Konhauser, Daniel Alessi and Murray Gingras. Noah Planavsky acknowledges the Packard Foundation and Lidya Tarhan the NASA Exobiology Program and a Yale University Postdoctoral Associateship.

References

Abdel-Fattah, Z.A., Gingras, M.K. & Pemberton, S.G. 2011: Significance of hypoburrow nodule formation associated with large biogenic sedimentary structures in open-marine bay siliciclastics of the Upper Eocene Birket Qarun Formation, Wadi El-Hitan, Fayum, Egypt. *Sedimentary Geology 233*, 111–128.

Alessi, D.S. & Fein, J.B. 2010: Cadmium adsorption to mixtures of soil components: testing the component additivity approach. *Chemical Geology 270*, 186–195.

Aller, R.C. 1983: The importance of the diffusive permeability of animal burrow linings in determining marine sediment chemistry. *Journal of Marine Research 41*, 299–322.

Borrok, D., Turner, B.F. & Fein, J.B. 2005: A universal surface complexation framework for modeling proton binding onto bacterial surfaces in geologic settings. *American Journal of Science 305*, 826–853.

Bosc, L.A.G. 1802: *Histoire naturelle des vers contenant leur description et leurs moeurs. Tome Premiere*. Chez Deterville, Paris, no. 16, pp. 142–143.

Coates, J. 2000: Interpretation of infrared spectra, a practical approach. *In* Meyers, R.A. & McKelvy, M.L. (eds): *Encyclopedia of Analytical Chemistry*, 10815–10837. Wiley, Chichester.

Fattom, A. & Shilo, M. 1984: Hydrophobicity as an adhesion mechanism of benthic cyanobacteria. *Applied and Environmental Microbiology 47*, 135–143.

Flynn, S.L., Gao, Q., Robbins, L.J., Warchola, T.J., Weston, J.N.J., Alam, M.S., Liu, Y., Konhauser, K.O. & Alessi, D.S. 2017: Measurements of bacterial mat metal binding capacity in alkaline and carbonate-rich systems. *Chemical Geology 451*, 17–24.

Gingras, M.K., Pemberton, S.G., Saunders, T. & Clifton, H.E. 1999: The ichnology of modern and Pleistocene brackish-water deposits at Willapa Bay, Washington: variability in estuarine settings. *Palaios 14*, 352–374.

von Gunten, K., Alam, M.S., Hubmann, M., Ok, Y.S., Konhauser, K.O. & Alessi, D.S. 2017: Modified sequential extraction for biochar and petroleum coke: metal release potential and its environmental implications. *Bioresource Technology 236*, 106–110.

Hao, W., Flynn, S.L., Alessi, D.S. & Konhauser, K.O. 2018: Change of point of zero net proton charge (pH_{PZNPC}) of clay minerals with ionic strength. *Chemical Geology 493*, 458–467.

Herbelin, A.L. & Westall, J.C. 1999: *FITEQL 4.0: A Computer Program for Determination of Chemical Equilibrium Constants from Experimental Data; Report 99-01*. Department of Chemistry, Oregon State University, Corvallis.

Konhauser, K.O. & Gingras, M.K. 2011: Are animal burrows a major sedimentary sink for metals? *Ichnos 18*, 144–146.

Lalonde, S.V., Dafoe, L.T., Pemberton, S.G., Gingras, M.K. & Konhauser, K.O. 2010: Investigating the geochemical impact of burrowing animals: proton and cadmium adsorption onto the mucus lining of Terebellid polychaete worms. *Chemical Geology 271*, 44–51.

Liu, Y., Alessi, D.S., Flynn, S., Alam, M.S., Hao, W., Gingras, M.K., Huzhang, Z. & Konhauser, K.O. 2018: Acid-base properties of kaolinite, montmorillonite, and illite. *Chemical Geology 483*, 191–200.

Mangum, C.P., Cox, C.D., Santos, S.L. & Rhodes, W.R. Jr 1968: Distribution and feeding in the onuphid polychaete *Diopatra cuprea* (Bosc). *Marine Biology 2*, 33–40.

McIlroy, D., Worden, R.H. & Needham, S.J. 2003: Faeces, clay minerals and reservoir potential. *Journal of the Geological Society of London 160*, 489–493.

Milne, C.J., Kinniburgh, D.G. & Tipping, E. 2001: Generic NICA-Donnan model parameters for proton binding by humic substances. *Environmental Science and Technology 35*, 2049–2059.

Mishra, B., Boyanov, M., Bunker, B.A., Kelly, S.D., Kemner, K.M. & Fein, J.B. 2010: High- and low-affinity binding sites for Cd on the bacterial cell walls of *Bacillus subtilis* and *Shewanella oneidensis*. *Geochimica et Cosmochimica Acta 74*, 4219–4233.

Myers, A.C. 1972: Tube-worm-sediment relationships of *Diopatra cuprea* (Polychaeta: Onuphidae). *Marine Biology 17*, 350–356.

Naumann, D. 2000: Infrared spectroscopy in microbiology. *In* Meyers, R.A. & Mantsch, H.H. (eds): *Encyclopedia of Analytical Chemistry*, 1–32. Wiley, Chichester.

Nell, R.M. & Fein, J.B. 2017: Influence of sulfhydryl sites on metal binding by bacteria. *Geochimica et Cosmochimica Acta 199*, 210–221.

Over, D.J. 1990: Trace metals in burrow walls and sediments, Georgia Bight, USA. *Ichnos 1*, 31–41.

Parks, G.A. 1965: The isoelectric points of solid oxides, solid hydroxides, and aqueous complex systems. *Chemical Reviews 65*, 177–198.

Petersen, K., Kristensen, E. & Bjerregaard, P. 1998: Influence of bioturbating animals on flux of cadmium into estuarine sediment. *Marine Environmental Research 45*, 403–415.

Petrash, D.A., Lalonde, S.V., Gingras, M.K. & Konhauser, K.O. 2011: A surrogate approach to studying the chemical reactivity of burrow mucous linings in marine sediments. *Palaios 26*, 594–600.

Phillips, T.M. & Lovell, C.R. 1999: Distributions of total and active bacteria in biofilms lining tubes of the onuphid polychaete *Diopatra cuprea*. *Marine Ecology Progress Series 183*, 169–178.

Phoenix, V.R., Adams, D.G. & Konhauser, K.O. 2000: Cyanobacterial viability during hydrothermal biomineralisation. *Chemical Geology 169*, 329–338.

Phoenix, V.R., Martinez, R.E., Konhauser, K.O. & Ferris, F.G. 2002: Characterization and implications of the cell surface reactivity of *Calothrix* sp. Strain KC97. *Applied and Environmental Microbiology 68*, 4827–4834.

Puigdomenech, I. 2006: *HYDRA (Hydrochemical Equilibrium-Constant Database) and MEDUSA (Make Equilibrium Diagrams Using Sophisticated Algorithms) Programs*. Royal Institute of Technology, Stockholm.

Sakai, K. 2015: *Routine Soil Analysis Using an Agilent 8800 ICP-QQQ*. Application note 5991-6409EN. Agilent Technologies, Hachioji, Japan, 8 pp.

Seilacher, A. 2007: *Trace Fossil Analysis*, 226 pp. Springer-Verlag, Berlin Heidelberg.

Sverjensky, D.A. & Sahai, N. 1996: Theoretical prediction of single-site surface-protonation equilibrium constants for oxides and silicates in water. *Geochimica et Cosmochimica Acta 60*, 3773–3797.

Vinn, O. 2013: Occurrence, formation and function of organic sheets in the mineral tube structures of Serpulidae (Polychaeta, Annelida). *PLoS ONE 8*, e75330.

Warchola, T.J., Flynn, S.L., Robbins, L.J., Liu, Y., Gauger, T., Kovalchuk, O., Alam, M.S., Wei, S., Myers, R., Bishop, B., Lalonde, S.V., Gingras, M.K., Kappler, A., Alessi, D.S. & Konhauser, K.O. 2017: Field- and lab-based potentiometric titrations of microbial mats from the Fairmont Hot Spring, Canada. *Geomicrobiology Journal 34*, 851–863.

Weckesser, J., Hofmann, K., Jurgens, U.J., Whitton, B.A. & Raffelsberger, B. 1988: Isolation and chemical analysis of the sheaths of the filamentous cyanobacteria *Calothrix parienta* and *C. scopulorum*. *Journal of general microbiology 134*, 629–634.

Yee, N. & Fein, J. 2001: Cd adsorption onto bacterial surfaces: a universal adsorption edge? *Geochimica et Cosmochimica Acta 65*, 2037–2042.

Yee, N., Benning, L.G., Phoenix, V.R. & Ferris, F.G. 2004: Characterization of metal-cyanobacteria sorption reactions: a combined macroscopic and infrared spectroscopic investigation. *Environmental Science & Technology 38*, 775–782.

Yu, Q., Szymanowski, J., Myneni, S.C.B. & Fein, J.B. 2014: Characterization of sulfhydryl sites within bacterial cell wall envelopes using selective site-blocking and potentiometric titrations. *Chemical Geology 373*, 50–58.

Zorn, M.E., Gingras, M.K. & Pemberton, S.G. 2010: Variation in burrow-wall micromorphologies of select intertidal invertebrates along the Pacific Northwest coast, USA; behavioral and diagenetic implications. *Palaios 25*, 59–72.

Supporting Information

Additional supporting information may be found online in the Supporting Information section at the end of the article.

Table S1. Measured masses (*m/z*), measurement modes, internal standards and calculated detection limits for the ICP-MS/MS measurements.